Materials Research Express

PAPER

Multi-scale analysis of fiber-matrix interfacial enhancement in hybrid structural composites with aligned zinc oxide nanowires

Materials Research Express

PAPER

Multi-scale analysis of fiber-matrix interfacial enhancement in hybrid structural composites with aligned zinc oxide nanowires

RECEIVED
27 February 2019

REVISED
5 April 2019

ACCEPTED FOR PUBLICATION
29 May 2019

PUBLISHED
7 June 2019

Parisa Marashizadeh, Mohammad Abshirini, Mrinal C Saha and Yingtao Liu

School of Aerospace and Mechanical Engineering, University of Oklahoma, Norman OK 73019 United States of America

E-mail: yingtao@ou.edu

Keywords: multi-scale analysis, zinc oxide nanowires, cohesive element, representative volume element

Abstract

In this paper, a three-dimensional multi-scale analysis is presented to investigate the interfacial properties and failure mechanism of an enhanced single carbon fiber reinforced polymer matrix composite under tensile load. Radially aligned zinc oxide (ZnO) nanowires on the surface of carbon fiber are simulated to evaluate the enhanced interfacial properties. At the micro-scale, the effective interfacial properties with various ZnO volume fractions are evaluated using an appropriate representative volume element. At the meso-scale, a cohesive zone model is used to study the interface between the fiber and the matrix. At the macro-scale, the first failure of the enhanced single fiber composite is evaluated utilizing the maximum tensile theory and an appropriate user subroutine in a finite element model. The developed multi-scale analysis demonstrates that the interfacial properties between carbon fibers and matrix can be improved by growing ZnO nanowires on the fibers' surface, resulting in enhanced stress transfer capability between matrix and fiber in structural composites.

1. Introduction

High-performance composite structures require reinforcement by fibrous materials with outstanding mechanical properties. Interfacial properties between fibers and matrix can significantly impact the overall performance of composites [1]. Poor interfacial adhesion can be caused by low surface energy, low contact area, chemically inert surface of the fiber, and manufacturing imperfections [2]. Inappropriate bonding between fiber and matrix leads to stress concentrations, resulting in early structural damage to composites, such as fiber pull-out, fiber breakage, and weak load-bearing characteristics. Therefore, the interfacial adhesion between the structural fibers and the polymer matrix is a determining factor of the mechanical interfacial strength of fiber-reinforced polymer matrix composites. Enhancing the interfacial properties and understanding their effects on stress transfer capabilities are critical for the design, development, and application of novel high-performance composite materials and structures.

Investigation of the interfacial properties and their effects on the adhesion between fiber and matrix in composites have attracted significant interests in the last decade. Single fiber fragmentation [3, 4] and nanoindentation [5, 6] are common experimental methods to characterize the interfacial strength in composites. Among various modeling approaches, the cohesive theory simulates the traction-separation of the adhesive region between fiber and matrix, leading to the evaluation of the mechanical properties of the interface [7, 8].

Due to the importance of the interfacial properties on the general quality of composites, various surface modification techniques, such as plasma modification [9] and surface functionalization [10], have been employed to improve the interfacial properties of carbon fiber reinforced composites. Nanostructured hybrid structural fiber can also improve interfacial behavior. For example, carbon nanotubes (CNTs) have been grown radially on the surface of carbon fibers to improve the mechanical and thermal properties of composites. In addition, a novel method to improve the interfacial properties is the synthesis of aligned zinc oxide (ZnO) nanowires on the surface of structural fibers [11–13]. The synthesis of ZnO nanorods on carbon fabric can

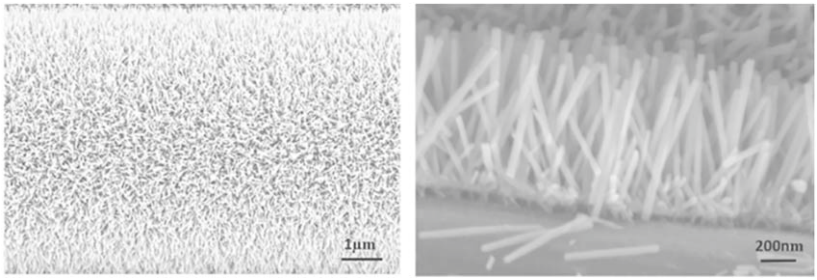

Figure 1. The SEM images of ZnO nanowires vertically aligned on the carbon fiber [16] (reproduced by permission from IOP).

increase the tensile and shear strength of the reinforced composites, partially due to the increased contact area between fiber and matrix [14]. Experimental studies have shown that ZnO nanowires can improve stress transfer to the fiber, causing earlier failure than the bare fibers [15]. Recently, synthesis and microstructural characterization of vertically aligned ZnO nanowires on carbon fiber was investigated by Wang *et al* [16]. Scanning electron microscopy (SEM) images of ZnO nanowires aligned on the carbon fiber are shown in figure 1.

In addition to experimental research, numerical simulations have been used to investigate the enhancement of mechanical properties of nanostructured fiber-reinforced composites at multiple length scales [17]. Kaminski investigated multi-scale homogenization of composites considering interface defects [18]. Kulkarni *et al* [19] reported that the effective material properties of nanocomposites with nanostructured hybrid fibers could be used to analyze fiber-matrix composites by considering a proper representative volume element (RVE). The effective thermal properties of the enhanced fiber structure considering radially grown CNTs on the surface of the fiber were explored by Kundalwal *et al* [20]. Recently, they explored the effective material properties of nano-reinforced composites with different CNT orientations on the carbon fibers using the molecular dynamics method [21]. To our best knowledge, no numerical analyses or modeling techniques have been reported to investigate the interfacial enhancement of ZnO nanowire reinforced hybrid composites and the improvement of load transferring to the fiber by modeling fiber failure under tensile loading.

In this study, a three dimensional (3D) multi-scale model is developed to simulate the single fiber fragmentation tests of ZnO nanowire enhanced carbon fiber composites. The numerical analysis of the hybrid composite with the enhanced interface between the fiber and matrix is implemented at the micro, meso, and macro-scales. The details of the multi-scale modeling are explained in section 2. The multi-scale modeling results and discussions of ZnO effects on interfacial properties of composites are addressed in section 3.

2. Multi-scale modeling of radially grown zinc oxide on carbon fiber

To enhance the interfacial properties of composites, ZnO nanowires have been grown radially on the surface of carbon fiber. The enhanced composite contains four phases: carbon fiber, interface, aligned ZnO nanowires/epoxy coating, and epoxy matrix. Due to the dramatic length-scale differences among the four phases, it is reasonable to develop a multi-scale model for the analyses of interfacial properties of the ZnO nanowires enhanced composites. The schematic of the developed multi-scale model is shown in figure 2. The aligned ZnO nanowires/epoxy coating can be investigated as an enhancement layer at the micro-scale to extract the effective properties of the nanostructure, as shown in figure 2(a). The arrangement of the radially grown nanowires on the fiber and the related micro-mathematical model is evaluated at the meso-scale and shown in figure 2(b). The cohesive zone model to simulate the interface between the fiber and the surrounding area is defined at this length scale, too. Finally, the failure analysis of the ZnO nanowires reinforced single carbon fiber in epoxy matrix under tensile load is conducted at the macro-scale and shown in figure 2(c).

The coordinate systems describing the orientation of ZnO nanowires and carbon fiber is shown in figure 2(d), where the lowercase letters represent the ZnO nanowire coordinate system and the capital letters are used to define the carbon fiber coordinate system. The nano-scale theoretical model provided by Chen *et al* [22] is used to estimate the material properties of the ZnO nanowires. According to this model, Young's modulus of the nanowires with the diameter of 500 nm and aspect ratio of ($l/d = 100$) is 120 GPa while the Poisson's ratio is 0.33 for this model.

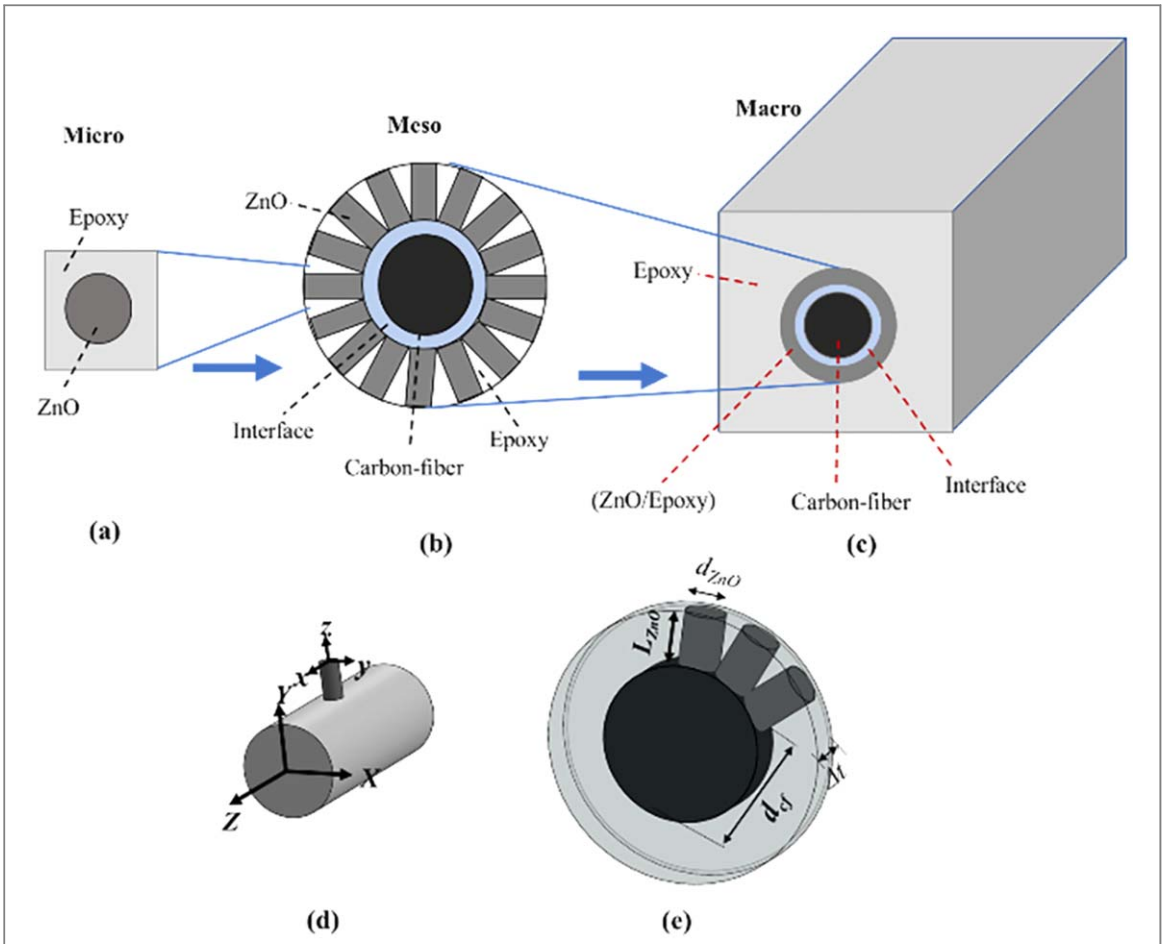

Figure 2. Schematic of multi-scale analysis (a) single ZnO nanowire embedded in epoxy, (b) ZnO nanowires radially grown on the fiber, (c) diverse phases containing fiber, interface, coating layer, and epoxy, (d) coordinate system for the ZnO and carbon fiber, (e) a unit cell for calculating the volume fraction of the ZnO with compact standing.

2.1. Micro-scale modeling of ZnO nanowires reinforced epoxy layer using RVE

Considering the ZnO nanowires as reinforcements embedded into the epoxy matrix, the spaces between the nanowires are filled with epoxy, creating a composite which can be investigated at the micro-scale. The volume fraction of ZnO nanowires in this layer is an important parameter for the estimation of the effective elastic properties of the coating layer. The maximum volume fraction of the ZnO nanowires can be calculated by minimizing the distance between ZnO nanowires on carbon fiber, resulting in the physical contact of the nearby nanowires, as shown in figure 2(e). By considering a ring-shaped volume element of ZnO/epoxy layer with thickness $\Delta t = d_{ZnO}$, inner diameter d_{cf}, and the outer diameter $d_{cf} + 2L_{ZnO}$, the maximum volume fraction of the ZnO in the composite can be calculated with equations (1) and (2).

$$\nu_{ZnO} = \frac{n_{ZnO}(V_{one\ ZnO})}{V_{composite}} \tag{1}$$

where n_{ZnO} is the total number of nanowires and V demonstrates the volume of the particles.

$$\nu_{ZnO} = \frac{\frac{\pi d_{cf}}{d_{ZnO}}\left(\pi\frac{d_{ZnO}^2}{4}L_{ZnO}\right)}{\pi[(R_{cf} + L_{ZnO})^2 - R_{cf}^2].d_{ZnO}} \tag{2}$$

For extracting the mechanical properties of the enhancement coating layer, it is common to explore a small RVE to reduce the computational cost. This small region should be chosen in such a way that it can represent the whole geometry so that its average properties can explain the general properties of the macroscopic system. Since the nanowires are grown radially and uniformly, as shown in figure 3(a), the ZnO/epoxy system encompasses a periodic unit cell. The unfolded cross-section of ZnO nanowire layer is shown in figure 3(b). The repeated RVE is chosen from this larger area as it is shown in figure 3(c).

To extract the effective mechanical properties of the ZnO/epoxy layer, the RVE is investigated based on continuum micromechanics assuming a perfect bonding between ZnO and epoxy. Various cross-sectional geometries for the epoxy matrix can be considered. However, it has been shown that a square cross-section RVE

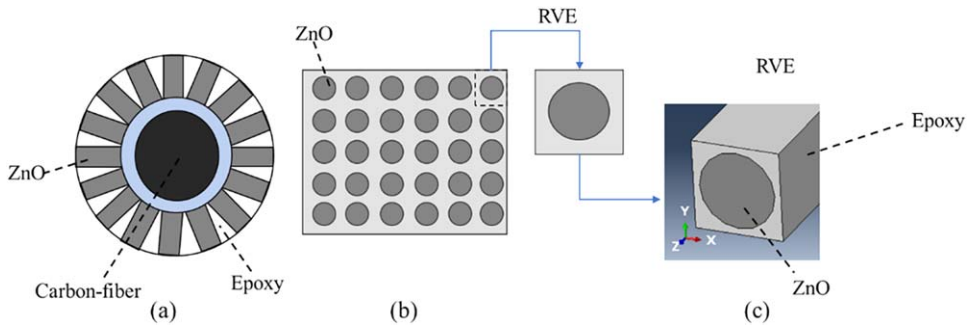

Figure 3. Extracting an RVE from the sample, (a) ZnO/epoxy coated the fiber, (b) unfolded view of the ZnO-epoxy layer, (c) RVE modeled in ABAQUS.

can result in more accurate effective elastic parameters [23]. Thus, this geometry is selected in this study as illustrated in figure 3(c). Generally, the three-dimensional stress-strain relation for an orthotropic material is defined by equation (3):

$$\{\varepsilon\}^{ij} = [S]^{ij}\ \{\sigma\}^{ij} \tag{3}$$

where $\{\varepsilon\}^{ij}$ and $\{\sigma\}^{ij}$ are the strain and stress vectors, respectively, and $[S]^{ij}$ is the elastic compliance matrix defined by equation (4) [24]:

$$[S]^{ij} = \begin{bmatrix} \frac{1}{E_{11}} & -\frac{\nu_{21}}{E_{22}} & -\frac{\nu_{31}}{E_{33}} & 0 & 0 & 0 \\ -\frac{\nu_{12}}{E_{11}} & \frac{1}{E_{22}} & -\frac{\nu_{32}}{E_{33}} & 0 & 0 & 0 \\ -\frac{\nu_{13}}{E_{11}} & -\frac{\nu_{23}}{E_{22}} & \frac{1}{E_{33}} & 0 & 0 & 0 \\ 0 & 0 & 0 & \frac{1}{G_{23}} & 0 & 0 \\ 0 & 0 & 0 & 0 & \frac{1}{G_{31}} & 0 \\ 0 & 0 & 0 & 0 & 0 & \frac{1}{G_{12}} \end{bmatrix} \tag{4}$$

where E_{ij}, G_{ij}, and ν_{ij} are Young's modulus, shear modulus, and Poisson's ratio of an orthotropic material in the ij directions, respectively. These nine constants define the mechanical properties of composite materials. The RVE can be modeled as a homogeneous orthotropic medium. Hence, the effective elastic modulus of the composite material can be determined by the homogenization of the material properties of the RVE. Accordingly, the average stress and strain of the composite material can be calculated with equations (5) and (6):

$$\overline{\sigma}_{ij} = \frac{1}{V_{RVE}} \int_V \sigma_{ij}(x, y, z)dV \tag{5}$$

$$\overline{\varepsilon}_{ij} = \frac{1}{V_{RVE}} \int_V \varepsilon_{ij}(x, y, z)dV \tag{6}$$

where V_{RVE} represents the volume of the RVE, and $\overline{\sigma}_{ij}$ and $\overline{\varepsilon}_{ij}$ are the average stress and strain of the RVE, respectively. The strain energy U^* stored in a heterogeneous RVE with the volume V_{RVE} is defined by equation (7):

$$U^* = \frac{1}{2} \int_V \sigma_{ij}\ \varepsilon_{ij} dV \tag{7}$$

Additionally, the total energy of a homogeneous RVE can be defined by equation (8):

$$U = \frac{1}{2} \overline{\sigma}_{ij}\ \overline{\varepsilon}_{ij}\ V_{RVE} \tag{8}$$

According to the strain energy equivalence principles, $U^* - U = 0$.

The nine constants of the elastic properties of RVE (equation (4)) can be extracted by applying different displacement and boundary conditions and using the strain energy equivalence principles [25]. Sun *et al* [26] provide further information about the continuum mechanics applied to calculate these parameters for a square

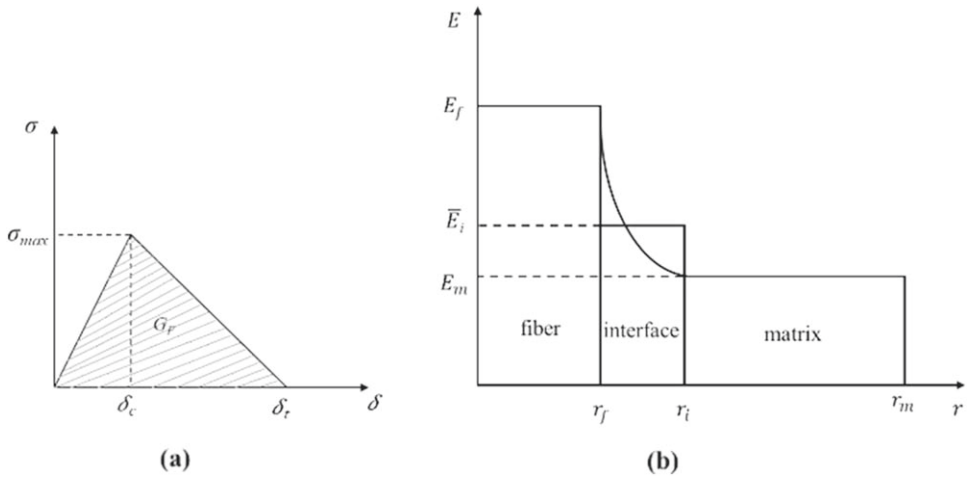

Figure 4. (a) Traction-separation behavior of the cohesive zone model, (b) Interface stiffness demonstration.

RVE. The FEM approach provided by Omairey *et al* [27] is used in this study to evaluate the effective elastic properties of the ZnO/Epoxy composite.

2.2. Meso-scale modeling using the cohesive zone model

In this paper, the cohesive zone model is used to define interfacial bonding between the fiber and matrix. The traction and separation of the interface can be represented through the cohesive zone. Different traction-separation laws, such as multi-linear, polynomial, and exponential, have been used in the literature to model the cohesive zone. The microstructural interface in both carbon/polymer and nanoparticle/polymer materials were properly modeled using the bilinear curve and verified with experimental results [28, 29]. Besides, This model has been widely used to simulate the cohesive zone model to explore progressive damage of carbon fiber/polymer composites and the single carbon fiber fragmentation test [30, 31]. The bilinear cohesive law is utilized in this study with the cohesive elements developed in ABAQUS. A thin annular layer is created between the fiber and matrix to model the interface. According to the cohesive model, traction across the bonded interface increases to a peak, then diminishing to model the decohesion as shown in figure 4(a) [32]. The elastic constitutive model to describe the mechanical behavior of the interface can be expressed via equation (9) [33].

$$t = \begin{Bmatrix} t_n \\ t_s \\ t_t \end{Bmatrix} = \begin{bmatrix} K_{nn} & K_{ns} & K_{nt} \\ K_{ns} & K_{ss} & K_{st} \\ K_{nt} & K_{st} & K_{tt} \end{bmatrix} \begin{Bmatrix} \delta_n \\ \delta_s \\ \delta_t \end{Bmatrix} = K\delta \tag{9}$$

where t is the traction of the interface, K is the cohesive stiffness, and δ is the separation displacement of the cohesive. The subscripts *nn*, *ss,* and *tt* denote the normal, shear and transverse directions, respectively. In this study, the stiffness is assumed to be constant in all three directions ($K_{nn} = K_{ss} = K_{tt} = K$). Proper surface contact is crucial to connect the interface to the neighboring components. Accordingly, a tie constraint is applied to the edges between the interface and epoxy, and between the interface and fiber [34].

Although cohesive stiffness plays an important role in defining the adhesive bonding of the interface, finding an accurate value requires empirical consideration, which leads to a range of values for a carbon/epoxy interface in the literature. Considering the issues related to the application of the empirical interface stiffness values, an assumption is introduced to calculate this value from a consistent approach in the case of bare and enhanced fibers. The effective interface stiffness (K) can be considered as the average elastic modulus of the interface ($\overline{E}_i$) across the thickness (t), which can be defined as equation (10) [35, 36]. The continuity condition of the modulus in this regime requires that ($E_i = E_f$ at $r = r_f$, $E_i = E_m$ at $r = r_i$). Based on the power law variation model ($E_i = Ar^{\beta}$) describing the interface stiffness along the radial distance shown in figure 4(b), the average Young's modulus of the interface can be defined as equation (11) [35, 37]. This equation is used in the rest of this paper to estimate the interface stiffness.

$$\overline{E}_i = \frac{1}{t}\int_{r_f}^{r_i} E_r(r)\,dr = \frac{1}{(r_i - r_f)}\int_{r_f}^{r_i} E_r(r)\,dr \tag{10}$$

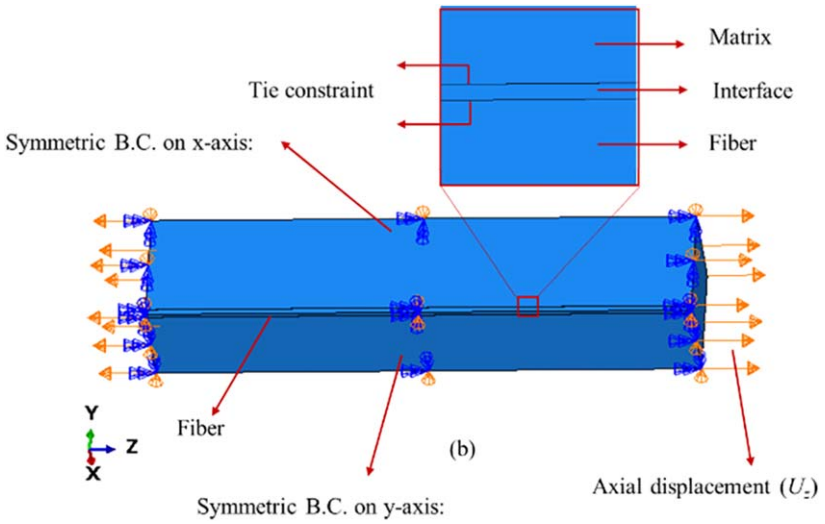

Figure 5. 3D FEM model of a single fiber reinforced with related boundary and loading condition.

$$\overline{E}_i = \frac{E_f r_f}{(r_i - r_f)(\beta + 1)}\left[\left(\frac{r_i}{r_f}\right)^{\beta+1} - 1\right]$$
$$A = \frac{E_f}{{r_f}^{\beta}};\ \beta = \frac{\ln E_m - \ln E_f}{\ln r_i - \ln r_f} \tag{11}$$

The area under the stress-displacement curve is the fracture energy (G_{IC}) obtained from the experiments, as shown in figure 4(a). The value of 100 J/m$_2$ is used for the G_{IC} in this analysis which is in the reported range for carbon fiber/epoxy (100–230 J/m$_2$ [38]). The damage criterion chosen for the traction-separation law is 'maximum nominal stress', where the damage initiates when the maximum nominal stress ratio is equal to one, as shown in equation (12):

$$\max\left\{\frac{t_n}{t_n^0}, \frac{t_s}{t_s^0}, \frac{t_t}{t_t^0}\right\} = 1, \tag{12}$$

where, t_n^0, t_s^0, and t_t^0 represent the maximum values of the nominal stress in the normal, first, and second shear direction, respectively. Since values between 40–60 have been suggested for these parameters for the carbon fiber/epoxy interface [30, 39], the nominal stress is assumed as 50 (MPa) in this study. Different interface thickness in the range of 0.01–0.4 μm have been reported in the literature for the carbon fiber reinforced epoxy (0.01 μm in [40], 0.1–0.2 μm in [41], 0.4 in [42]). Hence, various interface thickness in this range are used in this study to evaluate the effect of the cohesive zone thickness on the stress transferring to the fiber. The thin interface layer is modeled as a homogeneous material for simplicity.

2.3. Macro-scale FEM analysis of single carbon fiber in fragmentation test

A 3D FEM model of a single carbon fiber reinforced composite under tensile loading in a fragmentation test is simulated. Two types of FEM analyses including the single bare fiber in epoxy matrix composite and the enhanced single fiber with ZnO nanowire layer are conducted. To reduce the computational cost of the analysis, we take advantage of the symmetric geometry and boundary conditions of the model and consider only a quarter of the sample. The 3D FEM model with symmetric boundary conditions, relevant constraints, and applied axial load is shown in figure 5. The displacement in the x-axis (U_x), rotation around y and z-axis (UR_y, Ur_z) are zero on the x-symmetric plane, while for the y-symmetric plane $U_y = UR_y = UR_z = 0$. An 8-node linear brick 3D stress element with reduced integration and incompatible mode (C3D8I—an improved version of C3D8 elements) is used to model epoxy and carbon. An 8-node 3D cohesive element (COH3D8) is used to model the interface. More details about the elements used in this analysis can be found in [34]. The material properties of the different constituents of the model are described in table 1. The fiber diameter is 7 μm, the square cross-section of the epoxy matrix has a width of 140 μm, and the length of the model is 350 μm. By substituting the geometry parameters of the fiber and ZnO into equation (2), the maximum volume fraction of ZnO in the enhancement coating layer is calculated to be 57.84%.

Table 1. Material properties of fiber and matrix [22, 43].

Parameter	Value
Carbon fiber modulus (GPa)	232
Carbon fiber Poisson's ration	0.2
Carbon fiber tensile strength (GPa)	2.15
Epoxy modulus (GPa)	3.5
Epoxy Poisson's ratio	0.3
ZnO modulus (GPa)	120
ZnO Poisson's ratio	0.33

2.3.1. Damage modeling of the carbon fiber

Due to the brittle behavior of the carbon fiber, the maximum tensile strength theory is used to define the damage model on the fiber at the macro-scale. Based on this theory, the stress on the fiber is increased by raising applied displacement linearly up to the tensile strength of the material. If the stress exceeds its ultimate strength, the fiber breaks, and the stress drops. Hence, the fiber can be defined in two states, before failure (0) and after failure (1), with Young's modulus of the fiber defined by equation (13):

$$E_f = d.E_{cf} \tag{13}$$

where E_f is Young's modulus of the fiber for a specific state, d is the degradation factor, and E_{cf} is Young's modulus of the bulk carbon fiber. From damage modeling, the value of d can be taken to be 1 before failure, and it can be assumed to be small after fiber breakage. To avoid singular stiffness in any of the elements, the value of d after failure is considered to be 0.0001 in this study [43].

The damage model of the fiber can be simulated in ABAQUS using the USDFLD user subroutine [44]. This subroutine, programmed in FORTRAN, enables users to define the functional material properties of the modeled object. To use this algorithm, the filed variable (FV) defines the changes in the fiber's elastic modulus when the damage model is satisfied. The field variable is 0 if the maximum stress on the fiber is smaller than the fiber's strength and is 1 if it exceeds the fiber's strength. The FV and the solution-dependent state variable (SDV), which stores the information of the FV, can be obtained at each integration point to evaluate the damage model. In this regard, the GETVRM utility routine is used to call the maximum tensile stress on the fiber at each step and compare it to the fiber's strength. Finally, by updating the FVs to a point after failure, the damage algorithm is completed. This algorithm is diagrammed in figure 6.

3. Multi-scale modeling results of single carbon fiber fragmentation test

3.1. Single fiber composite with a bare carbon fiber

The modeling results of the single bare fiber fragmentation modeled using interfacial properties described in previous sections are presented here. Different loads are applied to the matrix, and the stress transferred to the fiber is obtained for each case. A mesh dependency analysis is first performed to investigate the sensitivity of the FEM response to the mesh density. Since the maximum stress on the fiber plays the most important role in the damage analysis, this parameter is considered to be the variable evaluated in each mesh density. Five different mesh sizes (figure 7) are implemented and the maximum stress as a result of an applied load of 1.2% strain is evaluated, as shown in figure 7(d). Three cases, with the total number of elements of 350 (course), 1160 (medium), and 14 040 (fine), are shown as examples in figures 7(a)–(c). The mesh size on the fiber is denser than the epoxy in all the cases due to the stress concentration in this zone. Since the model with 1440 elements shows no sensitivity to mesh refinement, it is used for the rest of the analysis.

In order to explore the effect of interface thickness on the micromechanical results, four typical interface thicknesses are implemented in the FEM, including 0.01, 0.2, 0.3, and 0.4 μm. The interface stiffness is calculated using equation (11) and the FEM model is updated for each thickness number. The samples are subjected to the 1.4% tensile strain and the maximum stress on the fiber is calculated for each model as shown in figure 8. It can be observed that although the interface stiffness is reducing slightly by increasing the thickness, the stress on the fiber is unchanged. Accordingly, the model used to simulate the interface is independent of the thickness. Hence, the arbitrary thickness of 0.01 μm is considered in the rest of the analysis.

By increasing the applied displacement, more load is transferred to the fiber, and the axial stress on the fiber increases. The stress distribution along the fiber length is obtained in four different strain. Figure 9(a) summarizes the results, showing that the stress at the two ends of the fiber is zero, and the maximum stress is in the center. It also proves that the stress in the fiber is enhancing by increasing the applied tensile load. When the

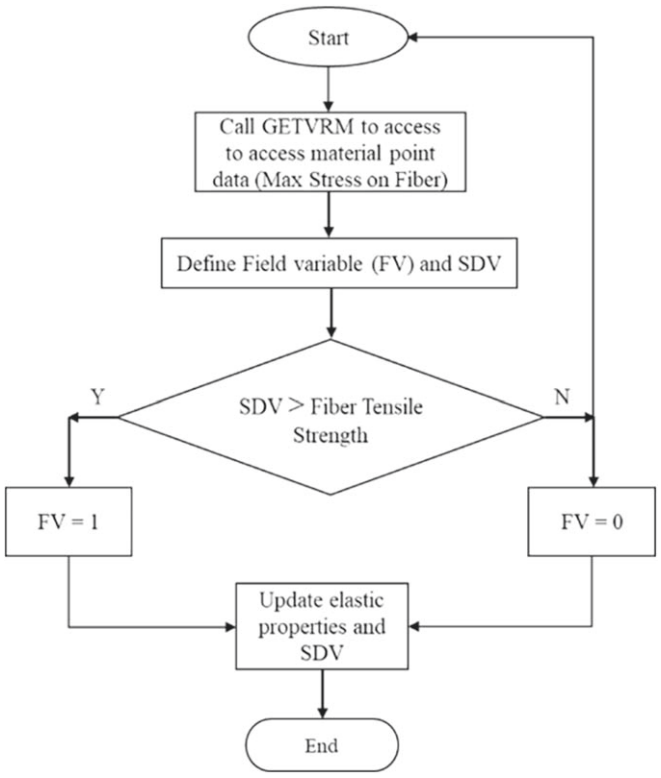

Figure 6. Flowchart of USDFLD subroutine and utility routine GETVRM.

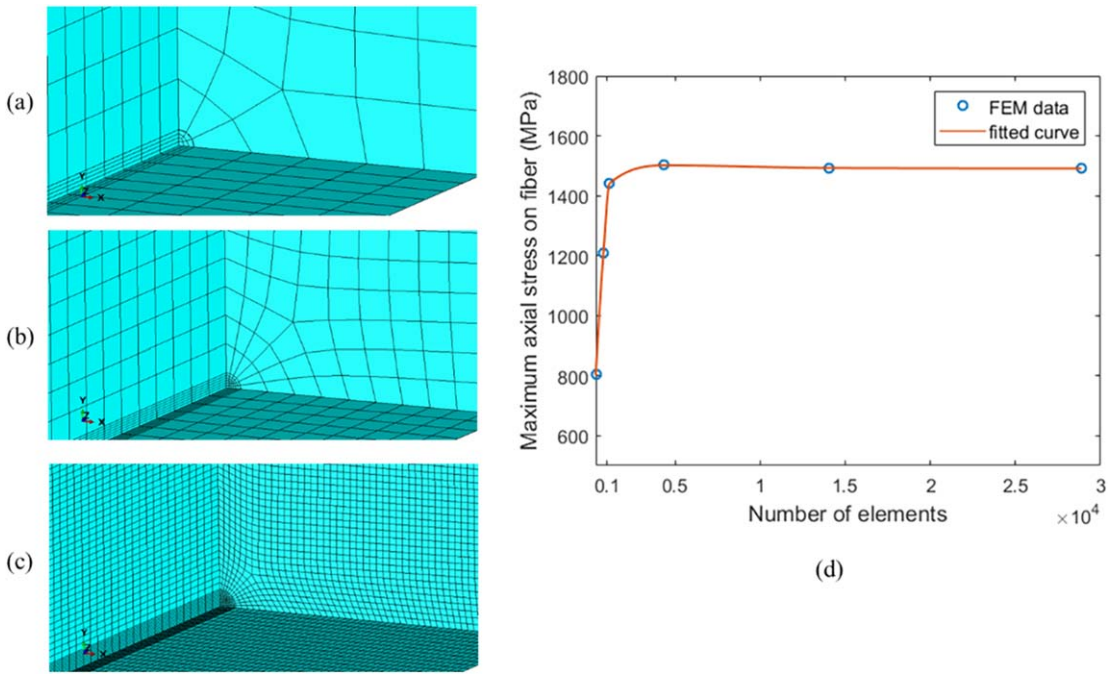

Figure 7. Mesh independency analysis of the FEM model: (a) coarse mesh, (b) medium mesh, (c) fine mesh, (d) sensitivity of the maximum stress on the fiber to the mesh density.

maximum stress reaches the strength of the fiber, failure occurs per the damage model explained in section 2.3.1, and the stress at the center of the fiber drops. The stress distribution on the fiber before and after the first fiber breakage is shown in figure 9(b). After breakage, the fiber is divided into two segments, with the maximum stress approximately at the center of each segment.

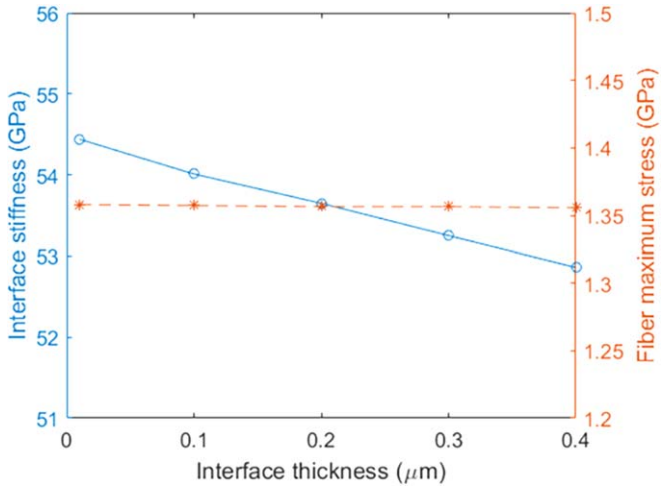

Figure 8. The effect of the Interface thickness on the maximum stress on the fiber.

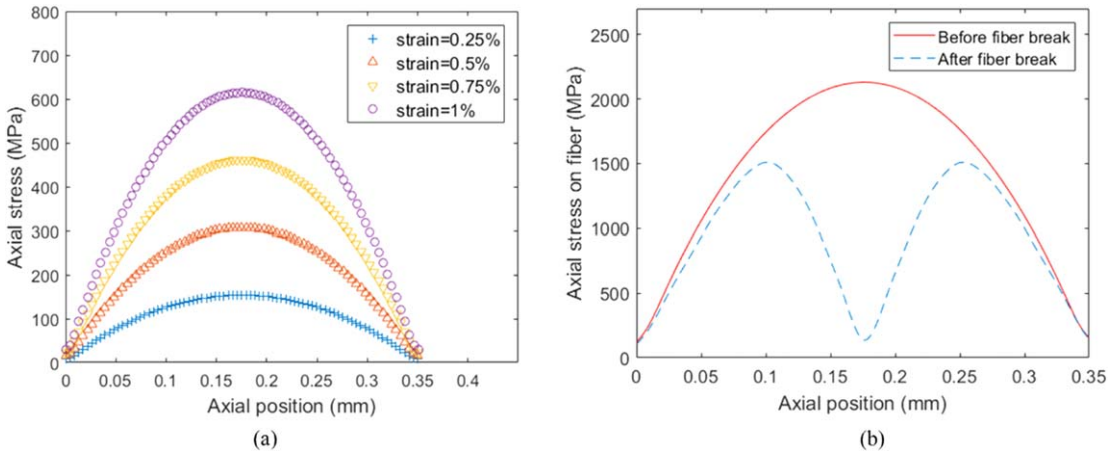

Figure 9. (a) Stress transferred to the fiber at different applied strains, (b) Stress distribution on the fiber before and after the break.

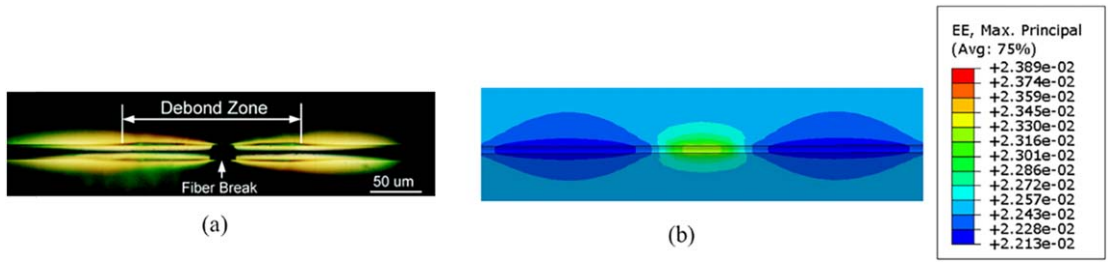

Figure 10. Strain re-distribution and the debonding area around the fiber break: (a) experimental [45] (reprinted by permission from Springer) and (b) FEM.

After the failure occurs, the stress/strain distribution in the matrix and interface at the region around the fracture tip is changed. This re-distribution causes debonding on both sides of the fiber fracture, which has also been observed in experiments. Kim and Nairn provided a photoelastic fringe pattern of the strain distribution and the debonded zone at the moment of failure of a fiber [45]. The strain re-distribution around the fracture zone obtained from the for the FEM in this study is compared with the experiment image shown in figure 10. The stress in the debonded zone of the matrix is larger than that in the neighboring regions.

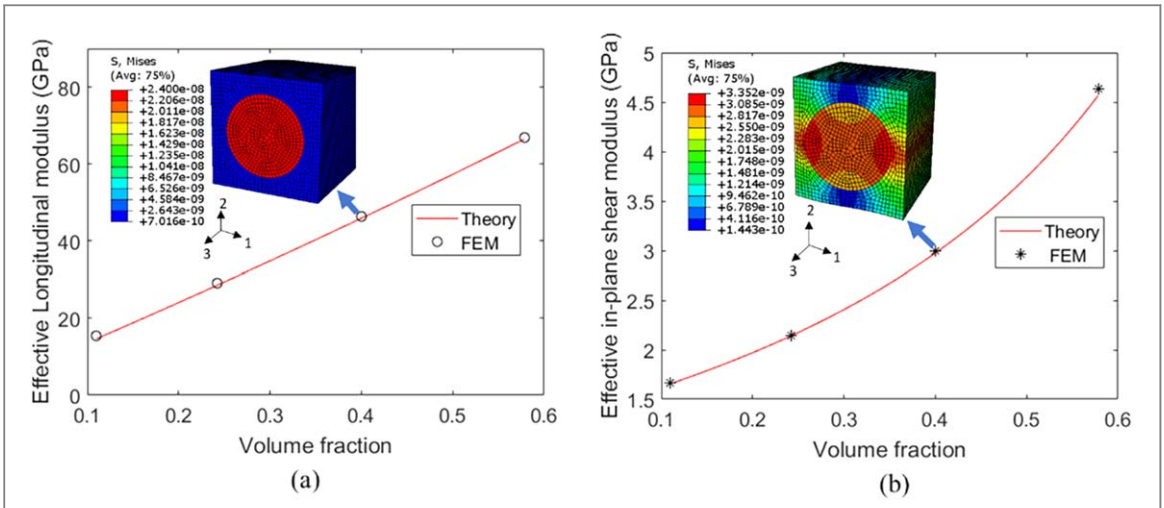

Figure 11. Comparison of the effective material properties of FEM and theory: (a) longitudinal modulus, (b) in-plane shear modulus.

3.2. Homogenization of the ZnO/epoxy layer

The effective elastic properties of the ZnO/epoxy layer with different ZnO volume fractions are estimated in this work via FEM analysis of the RVE. The homogenized structure is implemented as the coating layer of the enhanced fiber. Considering a constant ZnO diameter, the dimensions of the square RVE are derived and modeled in ABAQUS, as shown in figure 3(d). To verify the accuracy of the FEM calculated elastic parameters, the selected results are compared with the theoretical approach. According to the Halpin-Tsai mathematical model [46], the effective Longitudinal modulus (E_{L_c}) and in-plane shear modulus (G_{LT_c}) of the composite can be calculated using equations (14), (16), respectively.

$$\frac{E_{L_c}}{E_m} = \frac{1 + \eta_L \xi v_{ZnO}}{1 - \eta_L \xi v_{ZnO}} \tag{14}$$

$$\eta_L = \frac{\frac{E_{ZnO}}{E_m} - 1}{\frac{E_{ZnO}}{E_m} + \xi}; \ \xi = 2(l/d)_{ZnO} \tag{15}$$

$$\frac{G_{LT_c}}{G_m} = \frac{1 + \eta_G v_{ZnO}}{1 - \eta_G v_{ZnO}} \tag{16}$$

$$\eta_G = \frac{\frac{G_{ZnO}}{G_m} - 1}{\frac{G_{ZnO}}{G_m} + 1} \tag{17}$$

where E_{ZnO} and E_m are Young's modulus of the ZnO and epoxy, G_{ZnO} and G_m are the shear modulus of the ZnO and epoxy, v_{ZnO} is the volume fraction of the nanowires, and $(l/d)_{\mathrm{ZnO}}$ is the aspect ratio of the nanowires. The comparison of the theory and FEM results for the longitudinal and in-plane shear moduli of the ZnO/epoxy layer is shown in figure 11. This figure demonstrates that the FEM results and theory agree on the numerical accuracy of this property. The typical stress distribution on the RVE obtained from the homogenization analysis is also shown in this figure for $v_{\mathrm{ZnO}} = 0.24$.

It should be noted that the accuracy of the FEM is dependent on the quality of the meshing system. Accordingly, a sensitivity analysis is performed to find a proper mesh system which results in a minimum error when compared with the theory. The nine parameters of the elastic compliance matrix of the ZnO/epoxy composite (equation (4)) for four diverse ZnO volume fractions (11%, 24.24%, 15.67%, 57.84%) are shown in table 2. The calculated material properties are used as an input to investigate the ZnO nanowire enhanced carbon fiber. Using the relation between the coordinate systems of the ZnO/epoxy (figure 2(d)), where z is the longitudinal axis of the ZnO nanowire and Z is the longitudinal axis of the carbon fiber, appropriate material properties of the coating layer can be substituted for the next step.

3.3. Simulation results of ZnO nanowires enhanced carbon fiber in fragmentation tests

Using the extracted mechanical properties of the ZnO nanowire layer calculated in the previous section, the FEM model of the ZnO nanowire enhanced composites can be analyzed. To compare the behavior of composites using ZnO enhanced fiber with composites using only bare fiber under tensile load, the epoxy matrix, ZnO

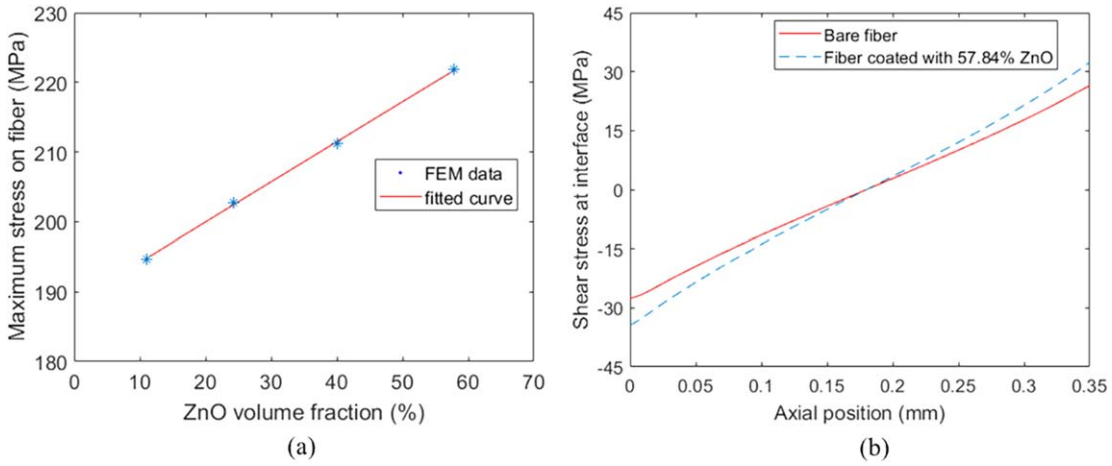

Figure 12. (a) Maximum stress transferred to the fiber at the applied strain of 0.2% for different volume fractions, (b) The shear stress at the interface for the bare fiber and the fiber coated with 57.84% ZnO at $\varepsilon = 0.8\%$.

Table 2. Effective material properties of ZnO/epoxy layer for the different volume fractions of ZnO.

Volume fraction of ZnO (%)	E_{11} (GPa)	E_{22} (GPa)	E_{33} (GPa)	G_{12} (GPa)	G_{13} (GPa)	G_{23} (GPa)	ν_{21}	ν_{23}	ν_{31}
11	4.462	4.462	15.548	1.571	1.657	1.661	0.381	0.083	0.304
24.24	5.787	5.787	29.184	1.876	2.143	2.14	0.362	0.056	0.309
40	8.348	8.348	46.474	2.362	2.993	2.991	0.309	0.053	0.314
57.84	14.034	14.025	67.008	3.367	4.687	4.635	0.228	0.063	0.32

nanowire enhanced carbon fiber, mesh properties, boundary conditions, and constraints of the new FEM model are kept the same as the bare fiber model.

After adding the ZnO/epoxy layer, the cohesive properties of the carbon fiber interface are calculated. As previously mentioned, according to equation (11), the magnitude of the cohesive stiffness (K) is proportional to the elastic properties of the fiber and the surrounding area. In the case of the ZnO nanowire enhanced carbon fiber, this parameter is directly proportional to the volume fraction of ZnO grown on the fiber surface, resulting in different interface properties. To investigate the effect of ZnO nanowire content on the on the load transferred to the fiber, four different ZnO volume fractions are considered, and a constant strain of 0.2% is applied to the model. The maximum stress on the fiber is calculated and shown in figure 12(a). Increasing the ZnO volume fraction enhances interfacial strength, resulting in an increase of maximum stress on the fiber.

The interfacial shear stress of the bare single fiber composite and the enhanced composite is evaluated. A comparison of the distribution of shear stress at the interface for the bare carbon fiber and fiber coated with 57.84% ZnO under the applied strain of 0.8% is illustrated in figure 12(b). This interfacial shear stress is the main principle of efficient stress transfer from the matrix to the fiber. According to this figure, the interfacial shear stress for the enhanced fiber is 25% larger than the bare fiber proving the interface enhancement.

It is expected that ZnO nanowire enhanced carbon fiber can improve interfacial bonding between fibers and matrix, resulting in increased load transfer capabilities in composites. To study this behavior, the USDFLD subroutine is used on the FEM model. The tensile strength of the fiber is assumed to be the same as the previous section, and a similar procedure for Young's modulus degradation after failure is performed. Increasing the applied displacement on the model results in higher maximum stress on the fiber. To show the effect of the interfacial enhancement on the first fracture of the fiber, the stress-strain of the enhanced carbon fiber, with the highest ZnO volume fraction considered (57.84%), is compared to that of the bare fiber, as shown in figure 13 (a). The value of the maximum stress is increased in the ZnO enhanced composites at any applied strain compared to the composites using bare fiber. Moreover, the first fiber fracture occurs at 2.1% tensile strain for the bare carbon fiber and at 1.73% tensile strain for the ZnO nanowire enhanced carbon fiber. These analyses show 21.4% reduction of failure strain due to the increased interfacial bonding between fiber and epoxy. The effect of ZnO volume fraction on the first failure strain of the carbon fiber is shown in figure 13(b). Composites using bare carbon fiber is represented by 0% volume fraction in this graph. The fracture strain is reduced whiling increasing ZnO volume fraction in the composites.

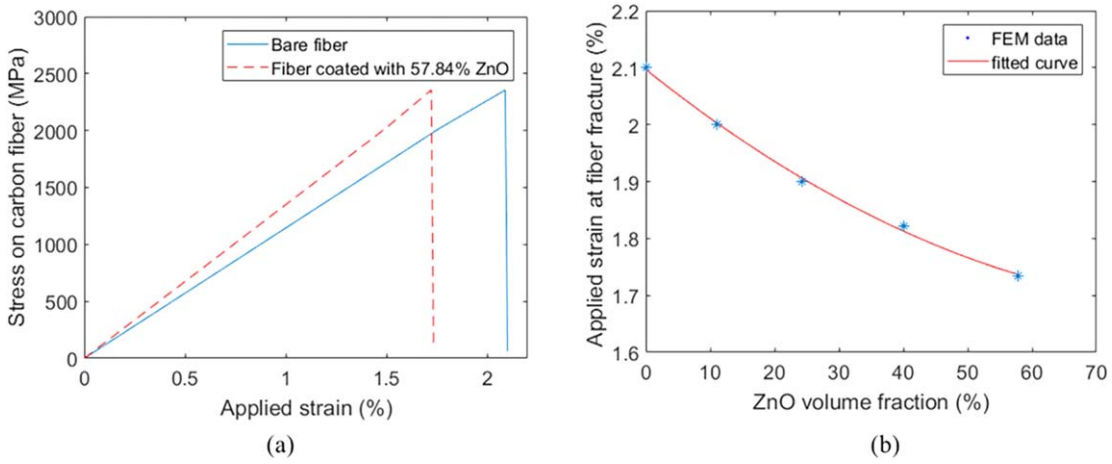

Figure 13. (a) Comparison of the maximum stress on the bare carbon fiber and the ZnO nanowire coated carbon fiber, (b) applied strain at the moment of fiber fracture for the different volume fraction of ZnO.

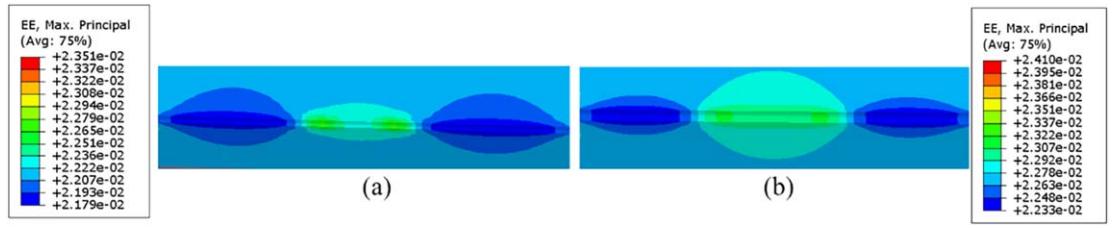

Figure 14. Comparison of the debonding zone on the strain distribution after fiber breakage for the (a) bare carbon fiber and (b) ZnO nanowire coated carbon fiber.

The effect of interfacial enhancement can also be observed by studying the strain re-distribution around the fracture zone. The debonded zone on the matrix, near the fracture tip, for the case of enhanced single fiber composite (57.84% ZnO volume fraction) and bare fiber composite are compared in figure 14. The debonded zone for the enhanced fiber is larger than for the bare fiber, as a result of higher interfacial strength. Similar results have been reported in experimental tests in which the stronger interface results in the larger debonded zone [47].

4. Conclusions

A multi-scale analysis of an enhanced fiber reinforced epoxy composite under tensile load is developed in this paper to analyze the effects of aligned ZnO nanowires on the improvement of the interface and the load transferring mechanism in composites. To investigate a four-phase hybrid composite (carbon fiber, interface, ZnO nanowires, and epoxy matrix), ZnO reinforced epoxy is considered as a coating layer and analyzed at the micro-scale. The mechanical properties of the coating layer are extracted by analysis of an RVE model. The results show a good agreement with the theory. The properties of the cohesive zone are explored at the meso-scale. It is shown that in the proposed model, the interface thickness has no influence on the maximum stress transferred to the fiber. The first fracture process of a bare single carbon fiber composite and ZnO nanowire enhanced carbon fiber is studied at the macro-scale using the damage theory of maximum stress modeled with USDFLD user subroutine. The results demonstrate that the assumption of fiber modulus degradation after reaching the axial strength can simulate the enhanced fiber failure properly.

The effect of interfacial stiffness on the load bearing of the fiber with various ZnO volume fraction is explored. Growing ZnO nanowires on the fiber create an interfacial layer with enhanced stiffness greater than the bare carbon fiber layer, resulting in interfacial bonding enhancement. The interfacial shear stress for the enhanced fiber is 25% larger than the bare fiber proving the interface enhancement. Under the same load condition, the maximum stress on the ZnO nanowire enhanced carbon fiber composites is larger than that of the

pure carbon fiber reinforced composites due to the improved interface between carbon fiber and epoxy matrix. The failure strain of a single fiber is reduced by 21.4% when the ZnO nanowires are grown on the fiber.

Acknowledgments

The authors appreciate the financial support from the National Science Foundation (award number: 1712178) and the SEED Funding for Interdisciplinary Research program in the Gallogly College of Engineering at the University of Oklahoma.

ORCID iDs

Yingtao Liu https://orcid.org/0000-0002-6232-9704

References

[1] Chand S 2000 Review carbon fibers for composites *J. Mater. Sci.* **35** 1303–13
[2] Bascom W D and Jensen R M 1986 Stress transfer in single fiber/resin tensile tests *The Journal of Adhesion* **19** 219–39
[3] Sørensen B F 2017 Micromechanical model of the single fiber fragmentation test *Mech. Mater.* **104** 38–48
[4] Seghini M, Touchard F, Sarasini F, Chocinski-Arnault L, Mellier D and Tirillò J 2018 Interfacial adhesion assessment in flax/epoxy and in flax/vinylester composites by single yarn fragmentation test: correlation with micro-CT analysis *Composites Part A: Applied Science and Manufacturing* **85** 1–8
[5] Li Q, Li Y and Zhou L 2017 Nanoscale evaluation of multi-layer interfacial mechanical properties of sisal fiber reinforced composites by nanoindentation technique *Compos. Sci. Technol.* **152** 211–21
[6] Teixeira R *et al* 2018 Nanoindentation study of the interfacial zone between cellulose fiber and cement matrix in extruded composites *Cem. Concr. Compos.* **85** 1–8
[7] Needleman A 1987 A continuum model for void nucleation by inclusion debonding *J. Appl. Mech.* **54** 525–31
[8] Mi Y, Crisfield M A, Davies G A O and Hellweg H B 1998 Progressive delamination using interface elements *J. Compos. Mater.* **32** 1246–72
[9] Cech V, Knob A, Lasota T, Lukes J and Drzal L 2017 Surface modification of glass fibers by oxidized plasma coatings to improve interfacial shear strength in GF/polyester composites *Polym. Compos.* **40** E186–E193
[10] Wang C *et al* 2017 Enhancing the interfacial strength of carbon fiber reinforced epoxy composites by green grafting of poly (oxypropylene) diamines *Composites Part A: Applied Science and Manufacturing* **99** 58–64
[11] Lin Y, Ehlert G and Sodano H A 2009 Increased interface strength in carbon fiber composites through a ZnO nanowire interphase *Adv. Funct. Mater.* **19** 2654–60
[12] Patterson B A, Galan U and Sodano H A 2015 Adhesive force measurement between HOPG and zinc oxide as an indicator for interfacial bonding of carbon fiber composites *ACS Applied Materials & Interfaces* **7** 15380–7
[13] Wang J, Weng B, Larson P and Liu Y 2018 Synthesis and characterization of self-assembled ZnO nanoarrays on hybrid structural fibers *Surfaces and Interfaces* (https://doi.org/10.1016/j.surfin.2018.10.006)
[14] Fei J, Luo D, Huang J, Zhang C, Duan X and Zhang L 2018 Growth of aligned ZnO nanorods on carbon fabric and its composite for superior mechanical and tribological performance *Surf. Coat. Technol.* **344** 433–40
[15] Zhang J, Yi D and Wang B 2017 Investigating the influence of ZnO nanowires on the interfacial micro-mechanical behavior of carbon fiber/epoxy microdroplet structures using micro-Raman spectroscopy *J. Mater. Sci.* **52** 3992–4001
[16] Wang J, Weng B, Larson P and Liu Y 2018 Synthesis of ZnO nanoarrays on carbon fibers using combined atomic layer deposition and hydrothermal methods *Mater. Res. Express* **5** 065029
[17] Salehi M, Marashizadeh P and Abshirini M 2015 Dynamic relaxation analysis of composite sandwich annular sector plate with viscoelastic core *Journal of Sandwich Structures & Materials* **17** 721–47
[18] Kamiński M 2005 Multiscale homogenization of n-component composites with semi-elliptical random interface defects *Int. J. Solids Struct.* **42** 3571–90
[19] Kulkarni M, Carnahan D, Kulkarni K, Qian D and Abot J L 2010 Elastic response of a carbon nanotube fiber reinforced polymeric composite: a numerical and experimental study *Composites Part B: Engineering* **41** 414–21
[20] Kundalwal S and Ray M 2014 Estimation of thermal conductivities of a novel fuzzy fiber reinforced composite *Int. J. Therm. Sci.* **76** 90–100
[21] Kundalwal S I and Meguid S A 2017 Multiscale modeling of regularly staggered carbon fibers embedded in nano-reinforced composites *European Journal of Mechanics—A/Solids* **64** 69–84
[22] Chen C, Shi Y, Zhang Y S, Zhu J and Yan Y 2006 Size dependence of Young's modulus in ZnO nanowires *Phys. Rev. Lett.* **96** 075505
[23] Chen X L and Liu Y J 2004 Square representative volume elements for evaluating the effective material properties of carbon nanotube-based composites *Comput. Mater. Sci.* **29** 1–11
[24] Jones R M 2014 *Mech. Compos. Mater.* (Boca Raton, FL: CRC Press)
[25] Liu Y J and Chen X L 2003 Evaluations of the effective material properties of carbon nanotube-based composites using a nanoscale representative volume element *Mech. Mater.* **35** 69–81
[26] Sun C T and Vaidya R S 1996 Prediction of composite properties from a representative volume element *Compos. Sci. Technol.* **56** 171–9
[27] Omairey S L, Dunning P D and Sriramula S 2018 Development of an ABAQUS plugin tool for periodic RVE homogenisation *Eng. Comput.* **35** 567–577
[28] Jiang L, Nath C, Samuel J and Kapoor S G 2014 Estimating the cohesive zone model parameters of carbon nanotube–polymer interface for machining simulations *J. Manuf. Sci. Eng.* **136** 031004
[29] Calzada K A, Kapoor S G, DeVor R E, Samuel J and Srivastava A K 2012 Modeling and interpretation of fiber orientation-based failure mechanisms in machining of carbon fiber-reinforced polymer composites *J. Manuf. Processes* **14** 141–9

[30] Wang L, Zheng C, Luo H, Wei S and Wei Z 2015 Continuum damage modeling and progressive failure analysis of carbon fiber/epoxy composite pressure vessel *Compos. Struct.* **134** 475–82
[31] Wang X, Zhang J, Wang Z, Liang W and Zhou L 2013 Finite element simulation of the failure process of single fiber composites considering interface properties *Composites Part B: Engineering* **45** 573–80
[32] Chandra N, Li H, Shet C and Ghonem H 2002 Some issues in the application of cohesive zone models for metal–ceramic interfaces *Int. J. Solids Struct.* **39** 2827–55
[33] Liu C, Zhou Z, Wang X and Zhang B 2012 Analysis and determination for the parameters of 'cohesive element' in the numerical model of single fiber composites: the elastic parameters *J. Reinf. Plast. Compos.* **31** 1127–35
[34] Hibbit H D, Karlsson B I and Sorensen E P 2012 ABAQUS user manual, version 6.12. Simulia, Providence, RI
[35] Yao Y, Chen S and Chen P 2013 The effect of a graded interphase on the mechanism of stress transfer in a fiber-reinforced composite *Mech. Mater.* **58** 35–54
[36] Wang J, Crouch S L and Mogilevskaya S G 2006 Numerical modeling of the elastic behavior of fiber-reinforced composites with inhomogeneous interphases *Compos. Sci. Technol.* **66** 1–18
[37] Qi G, Du S, Zhang B, Tang Z and Yu Y 2014 Evaluation of carbon fiber/epoxy interfacial strength in transverse fiber bundle composite: Experiment and multiscale failure modeling *Compos. Sci. Technol.* **105** 1–8
[38] Kim B W and Nairn J A 2002 Observations of fiber fracture and interfacial debonding phenomena using the fragmentation test in single fiber composites *J. Compos. Mater.* **36** 1825–58
[39] Jia Y Y, Yan W and Liu H Y 2011 *Numerical Study on Carbon Fibre Pullout Using a Cohesive Zone Model In Proceeding of 18th international conference on composite materials* 21–6
[40] Yang L, Wu Z, Cao Y and Yan Y 2015 Micromechanical modelling and simulation of unidirectional fibre-reinforced composite under shear loading *J. Reinf. Plast. Compos.* **34** 72–83
[41] Gu Y, Li M, Wang J and Zhang Z 2010 Characterization of the interphase in carbon fiber/polymer composites using a nanoscale dynamic mechanical imaging technique *Carbon* **48** 3229–35
[42] Garton A and Daly J H 1985 Characterization of the aramid: epoxy and carbon: epoxy interphases *Polym. Compos.* **6** 195–200
[43] Wang X, Zhang B, Du S, Wu Y and Sun X 2010 Numerical simulation of the fiber fragmentation process in single-fiber composites *Materials & Design (1980–2015)* **31** 2464–70
[44] Hibbitte K 2005 *Abaqus user Subroutines Reference Manual* (Hks Inc)
[45] Kim B W and Nairn J A 2002 Experimental verification of the effects of friction and residual stress on the analysis of interfacial debonding and toughness in single fiber composites *J. Mater. Sci.* **37** 3965–72
[46] Affdl J H and Kardos J 1976 The Halpin-Tsai equations: a review *Polymer Engineering & Science* **16** 344–52
[47] Feih S, Wonsyld K, Minzari D, Westermann P and Lilholt H 2004 *Testing Procedure for the Single Fiber Fragmentation Test* (Riso: Riso National Laboratory)